Spring Technical Meeting
of the Central States Section of the Combustion Institute
April 22–24, 2012

Quantitative Infrared Image Analysis Of Thermally-Thin Cellulose Surface Temperatures During Upstream and Downstream Microgravity Flame Spread From A Central Ignition Line

S.L. Olson[1], J. R. Lee[2], O. Fujita[3], M. Kikuchi[4], and T. Kashiwagi[5]*

[1]*NASA Glenn Research Center, Cleveland, OH*
[2]*QinetiQ North America, Cleveland, OH*
[3]*Hokkaido University, Sapporo, Japan*
[4]*JAXA, Tsukuba, Japan*
[5] *National Institute of Standards and Technology, Gaithersburg, MD*

Surface view calibrated infrared images of ignition and flame spread over a thin cellulose fuel were obtained at 30 Hz during microgravity flame spread tests in the 10 second Japan Microgravity Center (JAMIC). The tests also used a color video of the surface view and color images of the edge view using 35 mm 1600 Kodak Ektapress film at 2 Hz. The cellulose fuel samples (50% long fibers from lumi pine and 50% short fibers from birch) were made with an area density of 60 g/m^2. The samples were mounted in the center of a 12 cm wide by 16 cm tall flow duct that uses a downstream fan to draw the air through the flow duct. Samples were ignited after the experiment package was released using a straight hot wire across the center of the 7.5 cm wide by 14 cm long samples. One case, at 1 atmosphere 35%O_2 in N_2, at a forced flow of 10 cm/s, is presented here. In this case, as the test progresses, the single flame begins to separate into simultaneous upstream and downstream flames. Surface temperature profiles are evaluated as a function of time, and temperature gradients for upstream and downstream flame spread are measured. Flame spread rates from IR image data are compared to visible image spread rate data. IR blackbody temperatures are compared to surface thermocouple readings to evaluate the effective emissivity of the pyrolyzing surface. Preheat lengths are evaluated both upstream and downstream of the central ignition point. A surface energy balance estimates the net heat flux from the flame to the fuel surface along the length of the fuel.

Introduction

Microgravity flame spread over thin solid fuels has been a subject of considerable research over the past 30 years, and there have been significant advances in our understanding of the mechanisms of flame spread in microgravity [1, 2]. Notably, the roles of solid-phase radiative loss [3] and oxygen transport [4] on the microgravity extinction limits of solid fuels have been well established. Quantitative analysis of surface temperature profiles and net heat flux from the flame to the fuel has been challenging even in normal gravity experiments [5, 6]. Researchers have used thermocouples [7, 8] or holographic interferometry [9] in normal gravity, but only a few microgravity tests have

* Corresponding Author: Sandra L. Olson, NASA Glenn Research Center, 21000 Brookpark Rd. m.s. 77-5, Cleveland, OH 44135. Phone (216) 433-2859, Fax (216) 433-8050, email Sandra.L.Olson@NASA.gov

attempted to measure surface temperatures or heat flux [10-12]. Numerical models have been used to predict the net heat flux from the flame to the solid fuel [13-17].

There have been limited studies using infrared cameras in microgravity [18-21], most of which were of limited quantitative utility because of the early IR camera's 8 bit dynamic range. However, more advanced cameras have increased the bit depth, which improves the dynamic range enough to make the cameras useful for imaging surface heat up and pyrolysis during combustion experiments. In this work we present surface IR image results from microgravity combustion of cellulose fuels in different oxygen and flow environments. A previous paper [15] reported on visible flame spread results and compared the results to model predictions. The infrared surface temperature data reported here can provide added depth to the model comparisons.

Experimental Setup

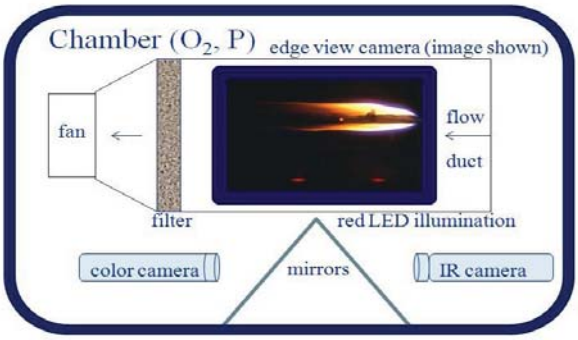

Figure 1: Conceptual schematic of experiment

The experimental hardware, shown conceptually in Figure 1, is described in [15], and consisted of a flow duct inside a sealed chamber was filled with 21%, 35%, or 50% oxygen in nitrogen at 1 atmosphere pressure. The flow duct provided a uniform flow of 5-20 cm/s past the fuel sample. The fuel samples were 60 mg/cm^2 cellulose 7.5 cm wide and 14 cm long. They were ignited with a straight hot wire across the center of the sample starting at time=0s (represented by the yellow dot in Figure 1). The flame was established by 2 seconds, so the data analysis begins at 2 seconds.

The infrared camera used in the tests was a 12 bit FLIR Systems, Inc. Prism DS™ with a 50 mm lens. A 200 nm bandwidth 'flame filter' centered at 3.8 μm was used to remove most of the gas-phase radiation from CO2 and H2O. The surface temperature calibration was performed with a calibrated Micron™ black body over the camera's operating range of 150^{o}C to 770^{o}C including the optical path elements (lens, calcium fluoride window, zinc sulfide window, 2 mirrors). A 10 pixel diameter area of the image was averaged to obtain the black body temperature to pixel level calibration. The accuracy of the black body surface temperatures is ±20^{o}C, and the spatial resolution was 0.3 mm per pixel. The IR camera image was 244 x 320 pixels, and the field of view was 7.5 cm wide by 10 cm long. The infrared images were analyzed using Tracer™ and Thermacam Researcher™ software.

A 35 mm color film camera was used to image the edge view of the flame during the test at ~ 2 frames per second, and a front view standard color video camera was used to image the surface view of the flame and fuel burning during the test. Type K thermocouples (0.005 cm diameter bare wire) were sewn into each sample to record the surface temperatures. The surface temperatures are used to compare to the black body temperature readings in order to get information on the fuel emissivity as it heats up and begins to pyrolyze. The surface thermocouple beads were located along the sample centerline at upstream locations +4 cm, +2 cm, 0 cm, and downstream -2 cm. [2]™

[2]™ Reference herein to any specific commercial product, process, or service by trade name, trademark, manufacturer, or otherwise, does not necessarily constitute or imply its endorsement, recommendation, or favoring by the United States Government or any agency thereof or its contractors or subcontractors.

Detailed Case Study

Tests were conducted at 21%, 35% and 50% oxygen molar concentrations and at 2, 5, 10, and 20 cm/s forced flow velocities. In this paper we analyze one case in detail – the 35% O_2, 10 cm/s case. This case is chosen because the flame is borderline for propagating simultaneously upstream and downstream. At lower oxygen and lower flow rates, the flame only propagates upstream.

An infrared still image for 35% O2, 10 cm/s forced flow is shown in Figure 2. The image is at 6 seconds into the drop test, while both upstream and downstream flames are still in the IR field of view. A color temperature legend is also shown. The printed grid on the sample is 1 cm square. It appears lighter in the infrared because its emissivity is higher than the pristine cellulose fuel. The thin diagonal wire is a thermocouple. The flame spread is reasonably two dimensional since the sample is wide enough and the ignition is uniform across the fuel width. A blue glow from gas-phase radiation is seen in the burnout gap, and is attributed to soot radiation.

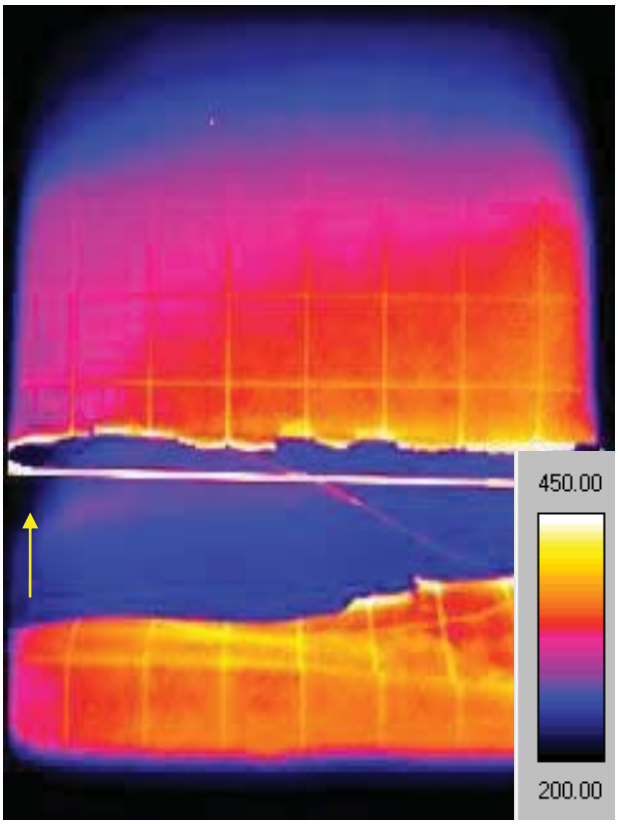

Figure 2: Infrared image from 35% O2, 10 cm/s forced flow microgravity flame spread test showing both upstream and downstream flame spread from a central ignition line. Color bar temperatures are in °C. Despite the flame filter, soot is visible in the burnout gap along with the igniter wire and fine wire TC.

The visible color flame images from the end of the test are shown in Figure 3 for the edge view (a) and surface view (b). The luminous upstream flame is robust, and the blue outer halo flame is visible in the edge view. The luminous flame fades as it extends downstream, and a kink in the flame shape is observed in the edge view near the location of the downstream fuel burnout edge (red dashed line in Fig. 3a). The outer blue halo flame fades before the kink, but there is a very faint blue inner flame visible in the left edge view flame that appears to be the beginning of a flame base attaching to the upstream edge of the downstream flame. The rest of the flame above the downstream side of the fuel has a large standoff distance and appears to still be an extension of the upstream flame. This is in contrast to a blue downstream flame fully separated from an upstream flame observed during a test at 35% O2, 20 cm/s flow (Fig.3c).

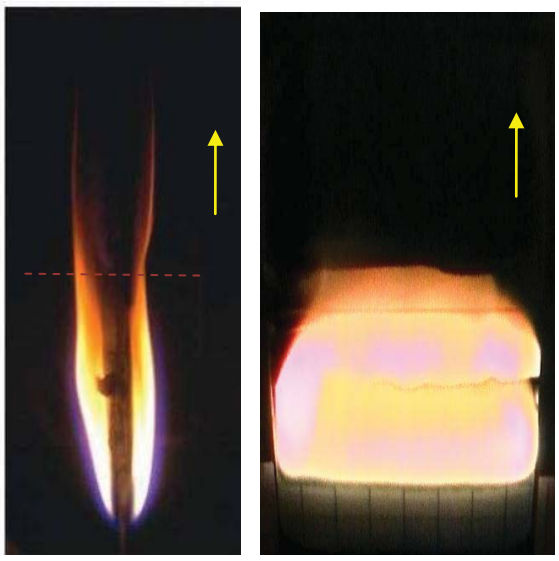

a) b)

3c)

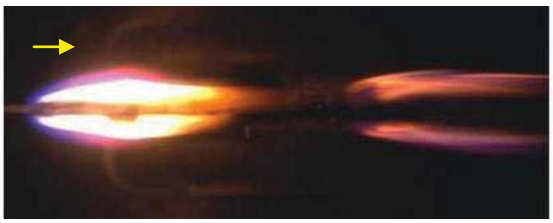

Figure 3: Visible flame images of the flame at the end of the test. a) edge view; b) front view; c) test at 35% O2, 20 cm/s with fully separated flames. Arrows indicate flow direction; dashed line indicates the incipient flame separation.

Blackbody surface temperature line profiles near the centerline down the length of the sample were taken every 0.5 second to study the transient surface temperature data. Figure 4 shows an example of the line profiles from a 35% O_2, 10 cm/s flow case. The igniter location is at 0 cm. Upstream of the igniter is positive x, and downstream of the igniter is negative x. The shaded box from 500K to 600K indicates where the temperature gradient data was evaluated. A linear regression fit provided an R2 value of at least 0.97 for all temperature gradient fits except for the downstream tests beyond 8 seconds. The later downstream data had few test points since most of the downstream sample was pyrolyzing by that point.

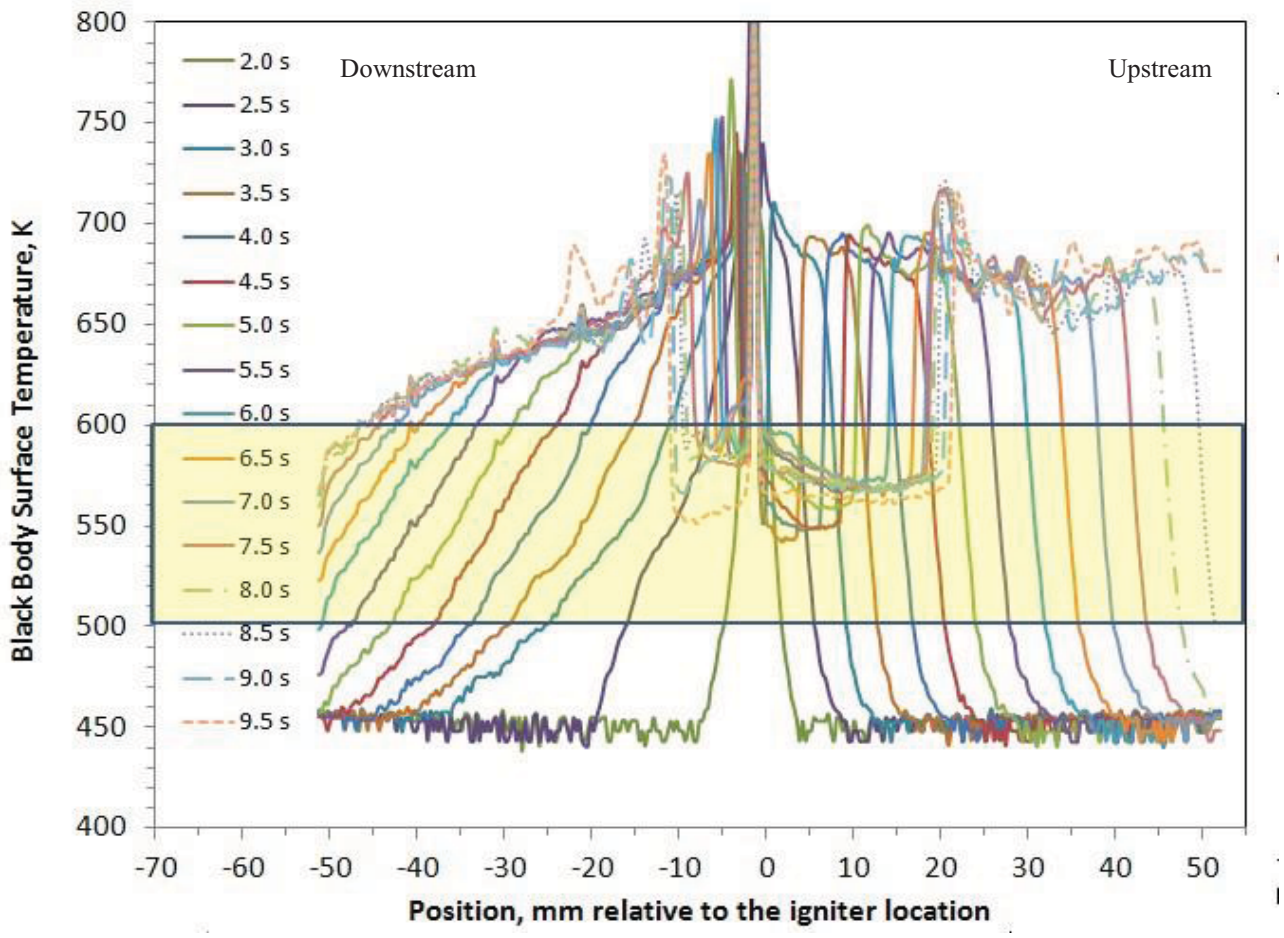

Figure 4: Blackbody surface temperature line profiles as a function of time for 35% O2, 10 cm/s test.

The surface temperature gradient as a function of time from this data is shown in Figure 5. Error bars on the temperature gradient are estimated to be ±10% of the gradient, based upon the 20°C accuracy of the camera and the 100°C range for the gradient evaluation. The upstream temperature gradient is a 53 K/mm after the ignition transient, and the downstream temperature gradient is a much lower 6.3 K/mm. This is almost an order of magnitude difference between the upstream flame and the downstream flame. The fuel beneath the upstream flame heats up quickly due to the intense heat flux from the leading edge of the flame, whereas the downstream flame has a large standoff distance since it is part of the upstream flame tail and not a truly separate flame during the test, as shown in Figure 3a.

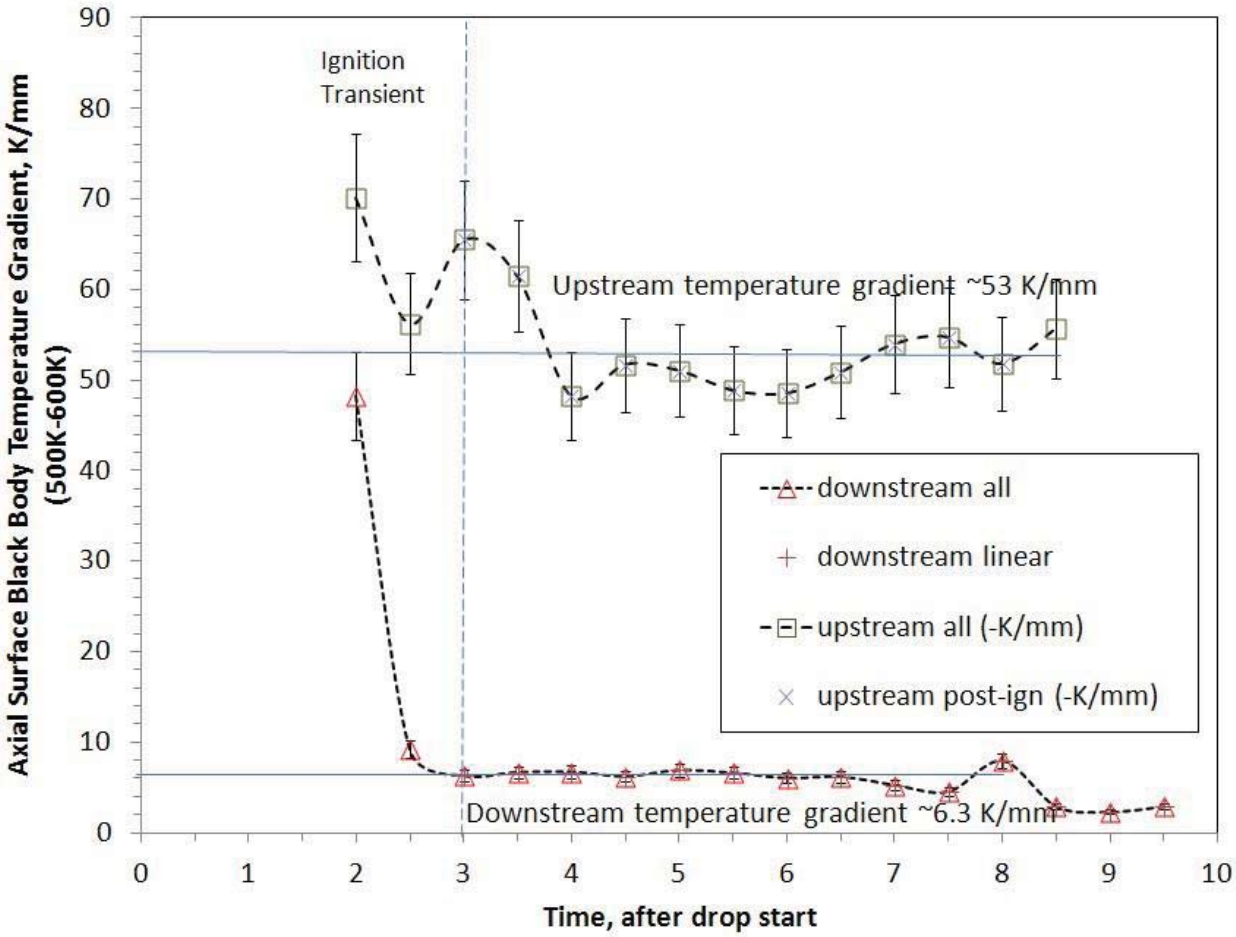

Figure 5: Temperature gradients for both upstream and downstream directions as a function of time during the microgravity drop.

The surface temperature can also be used to track the flame spread rate. To do this, we chose a surface temperature of 600K as a reasonable pyrolysis temperature. This worked well for the upstream flame spread, but the downstream flame spread required a higher temperature (700K) to detect the base (burnout) flame spread. Figure 6 shows the pyrolysis position versus time data. The upstream and downstream pyrolysis fronts (600K) spread at similar rates (7.6 mm/s and 8.2 mm/s, respectively) for most of the test. The upstream spread rate agrees well with the visible spread rate measurement of 7.4 mm/s, and the infrared measurement is expected to be more reliable since the visible flame is very luminous and increases in brightness as the test progresses and the burnout gap grows in time.

The downstream flame is growing throughout the test and may reach a steady state at approximately 7 seconds, as shown by the change in slopes of the 650K and 700K thermal fronts. The visible image after the test is complete, shown in Figure 7, reveals that the downstream sample is darkened but not to the point where the printed grid is no longer visible. The lines are visible from the 3rd downstream grid line (-30 mm). Temperatures at the 5th grid line (-50 mm) did not exceed 600K even though the sample continued to -70 mm (out of the IR field of view).

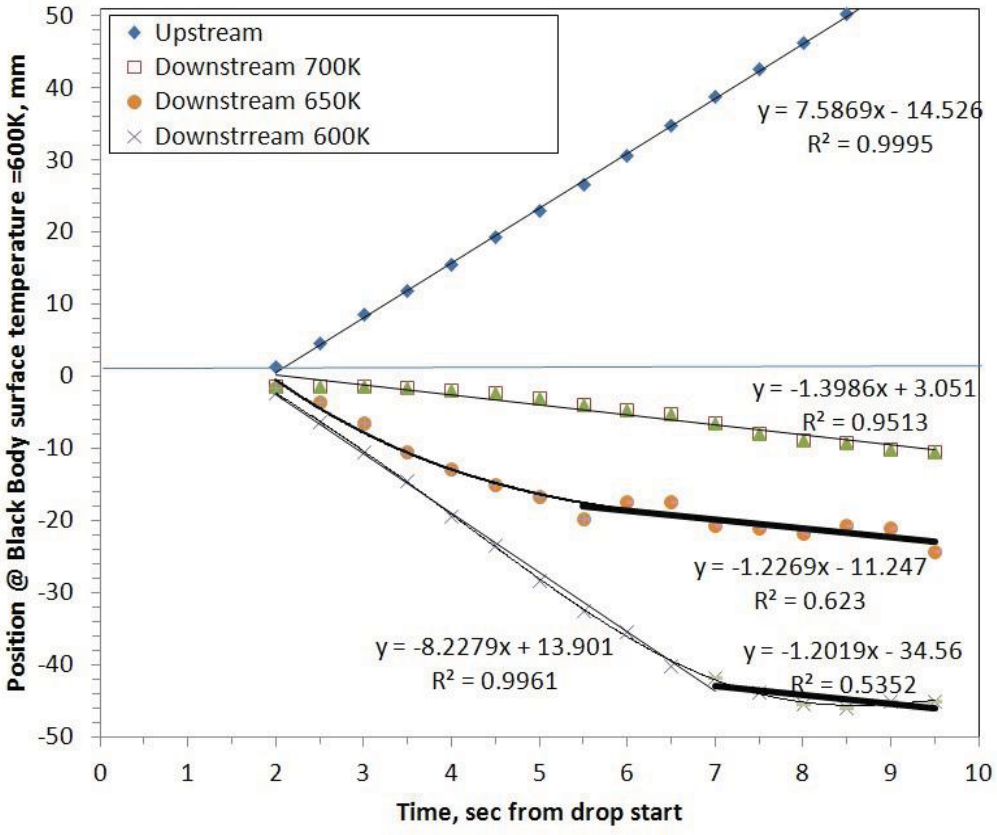

Figure 6: Position of the 600K, 650K, and 700K thermal wave as a function of time. Linear fits (shown) provide the flame or pyrolysis front spread rates.

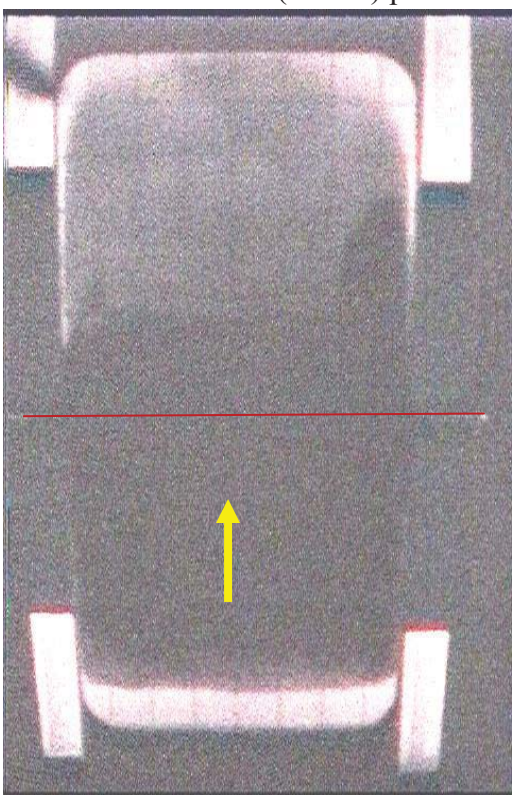

Figure 7: Charred sample surface post-test, with flow direction indicated with arrow. A very flat 2D upstream char front is shown within 1 cm of the upstream edge of the sample. Downstream of the igniter wire (red line) there is a fairly uniform darkening of the downstream sample for ~ 2 cm, and then a lighter darkening also to within 1 cm of the downstream end of the sample. The corners of the downstream sample are slightly less darkened, and the pattern shows a slight rounding for the outer 1.5cm. A quenching layer is visible along the edges of the downstream sample but not on the upstream sample. The dark zone at along the right side of the downstream sample is a crack in the pyrolyzed fuel.

Surface thermocouple data is compared with infrared blackbody temperatures at each surface thermocouple site. The IR data was taken at the same point for each frame (30 Hz) and compared with the thermocouple reading (20 Hz). The temperature traces are shown in Figure 8. The IR data plateaus at its minimum operating range temperature of 450K, but above that temperature the two sets of data agree well. The downstream IR data shows an early rise at 2.5 seconds that is attributed to ignition (gas phase radiation).

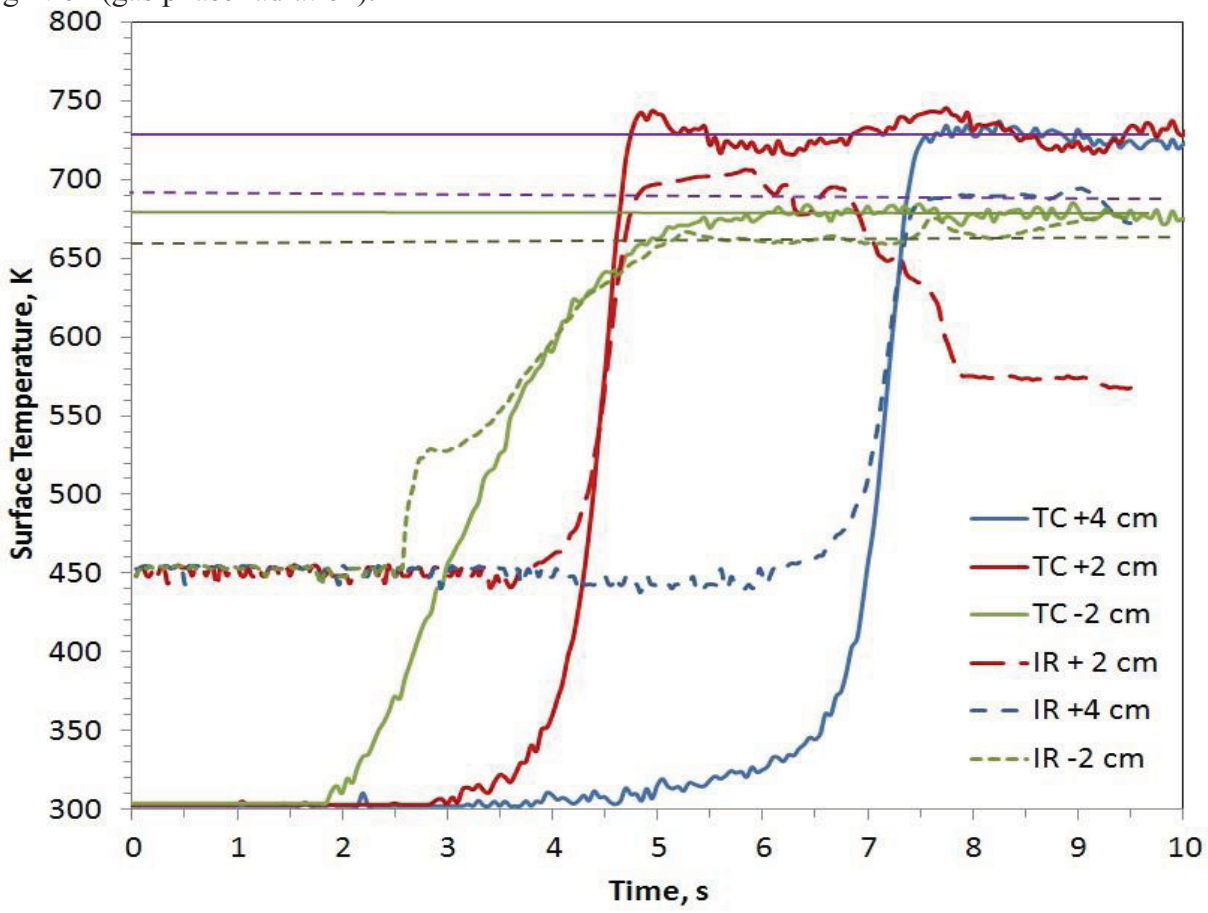

Figure 8: Infrared blackbody temperature data compared with thermocouple readings at 3 locations.

The steady state temperature plateaus (represented by the lines in the figure) at the pyrolysis temperature are taken to determine the pyrolyzing surface emissivity using:

$$\varepsilon = \frac{T_{IR}^4 - 300^4}{T_{TC}^4 - 300^4} \quad (1)$$

From the data in Fig. 8, T_{IR} = 690K and 660K and T_{TC}=730K and 680 K for the upstream and downstream flames, respectively. The estimated emissivities are 0.79 for the upstream charred fuel and 0.88 for the downstream charred fuel.

The preheat lengths for the flames can also be estimated by evaluating the length from 300K to 600K (ambient to pyrolysis temperatures), based upon the measured temperature gradients shown in Figure 5. The calculated preheat lengths are shown in Figure 9. The upstream flame has a steady preheat length of 6 mm throughout the test until the flame moves out of the IR camera field of view at 8.5 seconds. The downstream flame appears to reach a steady preheat length of ~46 mm until late in the test when the 600K line approaches the end of the fuel sample. However, as shown in Figure 6, the downstream burnout front (flame base) is represented by a much higher temperature (700K), so we also directly measure the distance between 600K and 700K, which is also shown in Figure 6, and reaches a steady length of ~36 mm later in the test. As shown in Figure 4, the temperature gradient is not linear over this range, so a direct measure is more representative. To estimate the total preheat length from ambient to burnout, we add the two pseudo-steady values to estimate a pseudo-steady preheat length of ~84 mm for the downstream flame, which is longer than the actual downstream sample (70 mm), so a steady-state concurrent flame size was not obtained for this test. This is not surprising, since the downstream flame never full separated from the upstream flame.

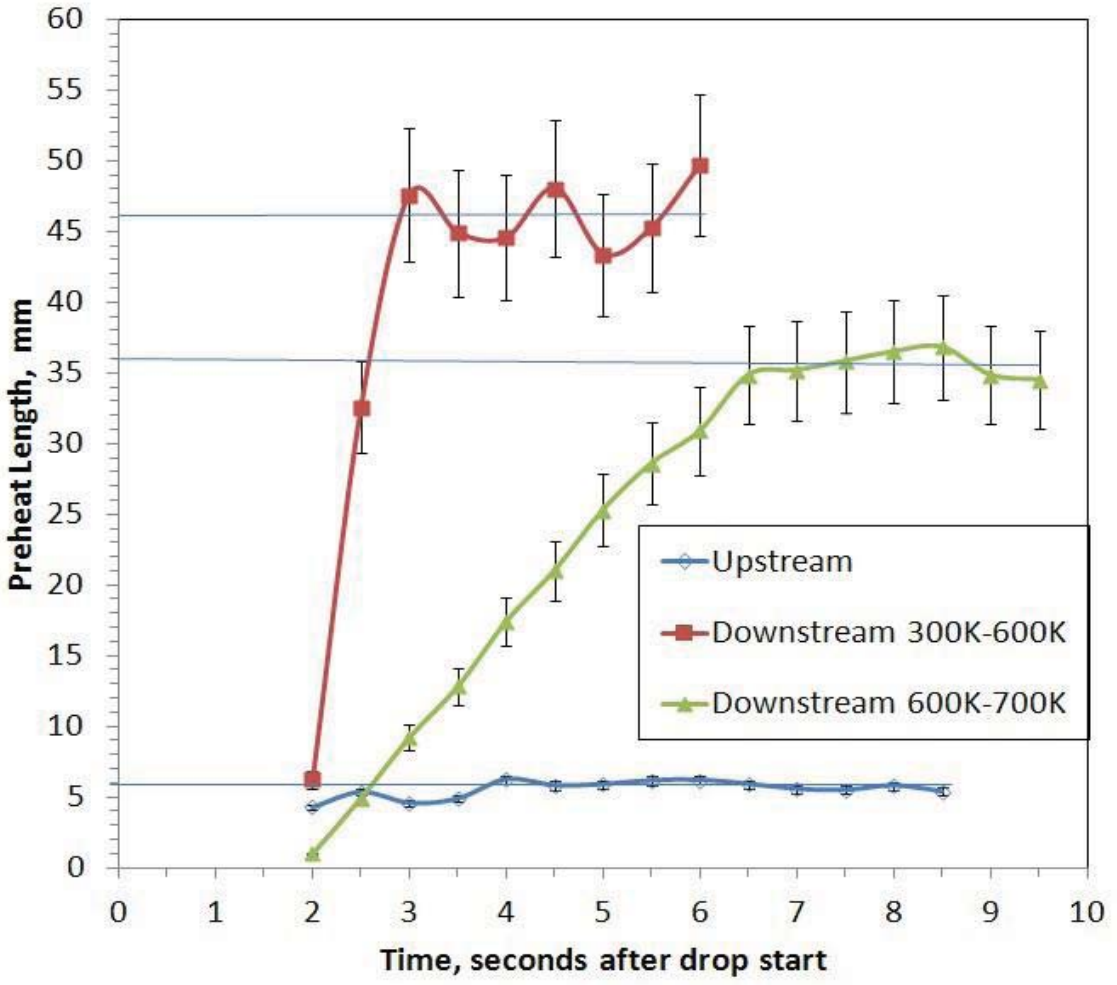

Figure 9: Preheat length as a function of time for 35% O2, 10 cm/s test.

A surface energy balance can be used to evaluate the net heat flux from the flame to the fuel surface, neglecting the heat of pyrolysis. The surface energy balance is

$$\dot{q}''_{netflame heat flux} = \rho_s \tau C_s \frac{\partial T_s}{\partial t} + \varepsilon\sigma(T_s^4 - T_\infty^4) \qquad (2)$$

Where $\rho_s\tau$ is the cellulose fuel half-area density of 0.003 g/cm^2, C_s is the fuel heat capacity, 1.26 J/g K, ε is the emissivity, which is unity for these black body temperature measurements, and σ is the Stefan-Boltzmann constant (5.729x10^{-12} W/cm^2). T_s is the blackbody surface temperature in K, and ambient temperature it 300K. The gradient in surface temperature is evaluated by simple difference over a 0.5 second interval at each pixel location along the line profile.

Figure 10 shows the resulting heat flux profile for the 35% O_2, 10 cm/s forced flow case. The profiles stop at ~0.2 W/cm^2 at the low end of the IR operating temperature range of ~450K. The upstream flame transitions from the ignition to a steady-state leading edge peak heat flux of ~2.4 W/cm^2. The downstream flame has a more complex heat flux profile, and neglecting the pyrolysis term is probably not a good assumption for this weak flame, which has a significant portion of the fuel surface above the pyrolysis temperature (~600K), as shown in Figure 4. With the shallow temperature gradient beneath the downstream flame, most of the flame's heat flux is re-radiated from the fuel surface. The peak heat flux for the downstream flame is at burnout at the flame base starting at 5 seconds, and it is generally lower than the upstream heat flux peak.

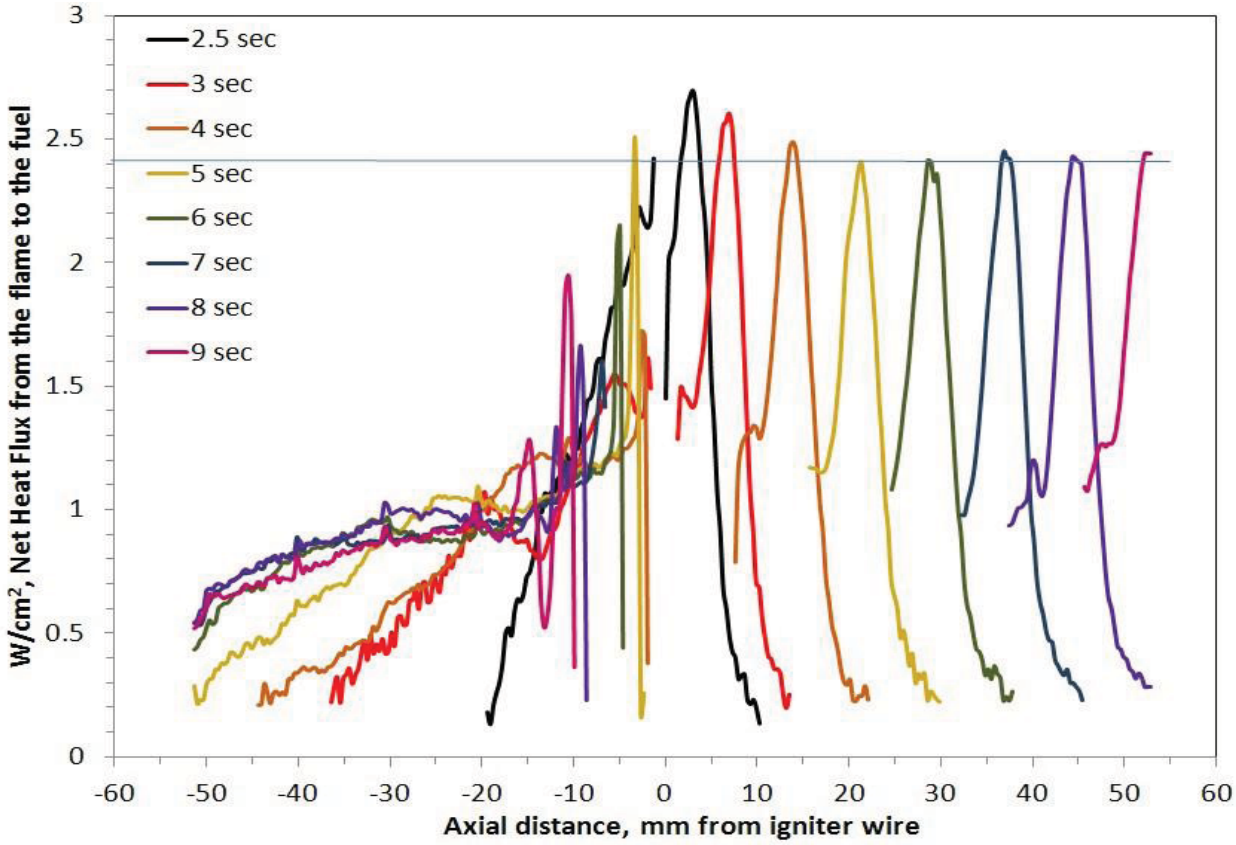

Figure 10: Flame heat feedback to the fuel surface based on the surface energy balance, Eq. (2).

Summary

The infrared surface temperature image data obtained during microgravity testing of cellulose ignition and flame spread have been analyzed to provide quantitative temperature gradients, preheat lengths, flame spread rates, and net flame heat flux to the fuel sample for both upstream and downstream flame spread. The case examined here is for a borderline simultaneous upstream-downstream flame spread, and highlights the differences in the strength of the two halves of the flame as they spread apart. A previous paper [15] reported on visible flame spread results and compared the results to model predictions. The infrared surface temperature data reported here can provide added depth to the model comparisons. The analysis results of this case are also obtained for other drop tests and will be reported in an upcoming journal article.

Acknowledgements

This work was jointly supported by a NASA/ NEDO international agreement. The microgravity experiments of this work were performed at JAMIC (Japan Microgravity Center) during March, 1999 under the management of JSUP (Japan Space Utilization Promotion Center) as a part of an R&D project of advanced combustion science utilizing microgravity by NEDO (New Energy and Industrial Technology Development Organization of Japan). The authors would like to thank NASA electrical engineer Mike Capelety and the NASA TIGER engineering team for supporting the rig buildup and testing. The authors would also like to thank Kenichi Ito, Katsuhiro Nishizawa and JAMIC facility personnel in performing the microgravity experiments.

References

1. Ross, H.D., ed. Microgravity Combustion: Fire in Free Fall, Academic Press, 2001.
2. Fernandez-Pello, A.C., Combustion Fundamentals of Fire, Chapter 2 “The Solid Phase”, Academic Press Limited, 1995.
3. T’ien, J. S., *Combust. Flame* 65:31–34 (1986).
4. Olson, S.L., *Combustion Science and Technology*, 76,4-6, pp. 233-249, 1991.
5. Hirano, T., and Saito, K.; *Prog. Energy Combust. Sci*. 20, 461-485, 1994.
6. Quintiere, J.G.; Fundamentals of Fire Phenomena, John Wiley and Sons Ltd., 2006.
7. Hirano, T., Noreikis, S.E., and Waterman, T.E.; *Combust. Flame* 23, 83-96, 1974.
8. Cordova, J.L., Walther, D.C., Torero, J.L., and Fernandez-Pello, A.C., Combust. Sci. and Tech. 164 (1) 253-278, 2001.
9. Ito, A., and Kashiwagi, T.; *Combust. Flame* 71, 189-204, 1988.
10. Bhattacharjee, S., Altenkirch, R.A., Olson, S.L., and Sotos, R.G.; J. Heat Transfer 113 (3), 670-676, 1991.
11. Olson, S.L., Kashiwagi, T., Fujita, O., Kikuchi, M., and Ito, K.; Combust. Flame 125, 852-864, 2001.
12. Olson, S.L., Hegde, U., Bhattacharjee, S., Deering, J.L. Tang, L., and Altenkirch, R.A.; Combust. Sci. and Tech. 176, 557-584, 2004.
13. Ferkul, P.V., and T’ien, J.S.; *Combust. Sci and Tech.* 99 345-370, 1994.
14. Di Blasi, *Combust. Flame* 100, 332-340, 1995.
15. Prasad, K., Nakamura, Y., Olson, S.L., Fujita, O., Nishizawa, K., Ito, K., and Kashiwagi, T., Proc. Comb. Inst. 29 (2002) 2553-2560.
16. Nakamura, Y., Kashiwagi, T., McGrattan, K.B., and Baum, H.R.; Combust. Flame 130, 307-321, 2002.
17. Kumar, A., Shih, H.-Y., and T’ien, J.S.; Combust. Flame 132, 667-677, 2003.
18. Sanchez-Tarifa, C. and Lazaro, B., First International Symposium on Microgravity Research and Applications on Physical Sciences and Biotechnology, 2000.
19. H. D. Ross and F. J. Miller. *Twenty-sixth International Symposium on Combustion*, 1327–1334. Combustion Institute, 1996.
20. Feier, I. I., Shih, H.-Y., Sacksteder, K.R., and T’ien, J.S.; Proc. Comb. Inst. 29 (2002), 2569-2577.
21. Kleinhenz, J., Ferkul, P., Pettegrew, R., Sacksteder, K.R., and T’ien, J.S.; Fire & Materials 29 (2005), 27-37.